

Non-chiral ephemeral edge states and cascading of exceptional points in the non-reciprocal Haldane model

Aditi A. Prabhudesai,* H. S. Chhabra,* and Suraj S. Hegde†

Indian Institute of Science Education and Research,

Thiruvananthapuram

Kerala, India

(Dated: February 16, 2026)

We study a variant of the Haldane honeycomb model that has non-reciprocal hoppings between the next-nearest neighbours. The system on a torus hosts time-reversal symmetry protected ‘exceptional rings’(ER) in the spectrum. The ERs act as Berry-curvature flux tubes i.e the Berry curvature is non-zero only inside the ERs. The system on a cylinder having zig-zag boundaries (and transverse momentum k_x) hosts edge-states that have zero group velocity at $k_x = \pi$ and are therefore ‘non-chiral’. The edge states undergo a bifurcation transition at an exceptional point(EP)in the BZ and delocalise into the bulk. As the non-reciprocity is increased, the bulk states that are approaching each other are converted into pairs of EPs due to non-Hermiticity. As the non-reciprocity is further increased, there is a ‘Russian doll’-like nested proliferation of pairs of EPs, leading to an EP-cascade. The proliferation of EPs takes place only at specific values of the non-hermiticity parameter, leading to a step-like structure in the EP-pair density when plotted as a function of non-Hermiticity. Further, using wave packet dynamics, we find a tunable regime where the non-chiral edge states can be dynamically stabilised for large timescales. The ‘self-acceleration’ term in the equations of motion tends to diffuse the wave packets into the bulk, thus making them ‘ephemeral edge states’. But we find that for small non-hermiticity, the edge localisation is stabilised until late times for sufficiently wider wave packets. Thus, we have brought forth an intriguing phenomenology of the exceptional phase of the non-reciprocal Haldane model, which may bear direct relevance for systems such as disordered Kitaev honeycomb model, wherein such ERs have been predicted.

I. INTRODUCTION

Non-Hermitian operators or matrices appear in a variety of physical contexts such as optical/photonic systems, open quantum systems, disordered and interacting many-body systems, active matter etc [1–9]. Specifically, the spectral properties of such non-Hermitian operators play a crucial role in the effective descriptions of damping/dissipative evolutions or in determining the Green’s function properties [10–17]. There have been extensive studies on ‘non-Hermitian Hamiltonians’ themselves as objects of inherent interest, in order to investigate various kinds of phenomena such as exceptional points, spectral topology, non-Hermitian skin effect, lasing and unconventional bulk-boundary correspondence [2, 3, 7, 18]. There have been various experimental settings in which such non-Hermitian Hamiltonian based phenomena have been realised [19–24]. One of the ways in which non-Hermiticity enters into the description is through non-reciprocity of tunneling or interactions.

In this work, we study a non-Hermitian variant of the Haldane model, where the nearest neighbour (NN) hoppings are same as that of Haldane model but the next-nearest neighbour (NNN) hoppings have been modified with non-reciprocity. Haldane proposed a paradigmatic tight-binding model on a honey-comb lattice that hosts a topological phase with chiral edge states [25]. The

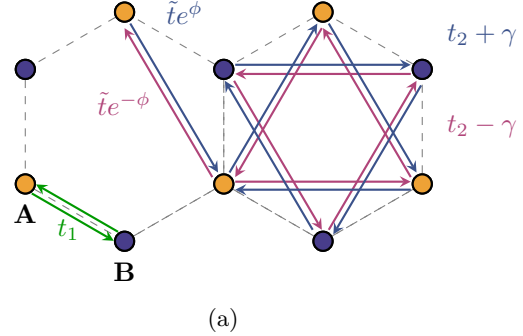


FIG. 1: Non-Hermitian Haldane model on a honeycomb lattice geometry with NN hopping and non-reciprocal NNN hopping amplitudes. The non-reciprocal hoppings can be expressed as hopping in the presence of a imaginary flux.

Haldane model introduces a phase in the NNN hoppings thus making them complex. However, Hermiticity of the Hamiltonian is retained by respecting reciprocity in the hopping amplitudes between any two sites. The phase was introduced by Haldane mainly to break the time-reversal symmetry and to obtain a ground state with a non-trivial Chern number. Here we introduce non-reciprocal NNN hopping rendering the Hamiltonian to be non-Hermitian and restoring time-reversal symmetry(TRS). Several works have studied various non Hermitian versions of the Haldane model including but

* These authors contributed equally to this work.

† surajh@iisertvm.ac.in

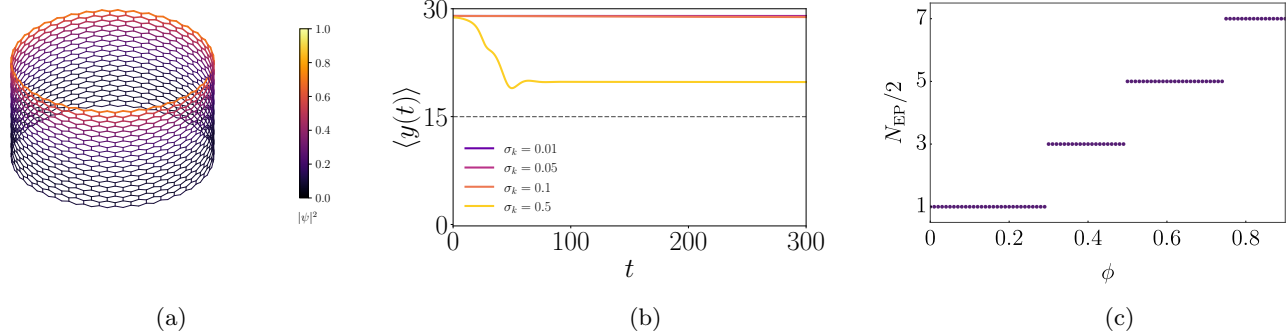


FIG. 2: (a) Non-chiral edge states in the imaginary-flux Haldane model. The edge-state wavefunction is obtained from diagonalising the lattice Hamiltonian over cylinder geometry with parameters $N_x = 40$, $N_y = 20$, $t_1 = 1.0$, $\tilde{t} = 0.3$, $\phi = 0.1$. (b) Dynamics of the wave packet expectation value $\langle y(t) \rangle$, illustrating late-time stabilisation at the edge for small non-Hermiticity ($\phi=0.05$) and for a range of wave packet widths. For larger widths, there is an edge-to-bulk diffusion due to ‘self-acceleration’ in wave packet equations of motion. (c) Step-like structure in proliferation of exceptional-point (EP) pairs as a function of the non-Hermiticity parameter ϕ for $N_y = 30$ and $\tilde{t} = 0.3$. The EP pairs appear at certain ‘critical’ values of ϕ , when pairs of bulk states tend to become degenerate. This leads to a jump in the number of EP pairs.

not restricted to non-reciprocal NNN hoppings [26–34]. Exceptional points(EPs) where both eigenvalues and the eigenvectors coalasce, are unique to non-Hermitian systems[35]. A key aspect of our model is the occurrence of the Exceptional Rings(ERs), a compact locus of EPs. There have been many studies on various intriguing properties of the ERs, such as topology, drumhead states, Fermi-ribbon states in both two and three dimensional systems [36–53]. The non-reciprocal Haldane model that we consider here is an explicit lattice realisation of TRS protected ER in two dimensions, while most other works concern a continuum model. Further, it has also been shown that such a non-hermitian Haldane model of Majorana fermions with an ER appears in the effective description of disordered spin liquids in the Kitaev honeycomb model[54]. Also, ERs have been shown to produce non-linear Hall responses coming from the Berry-curvature dipole [53]. This motivates us to study this model in further depth, particularly focusing on the EP properties and the edge phenomenology in the presence of boundaries.

We particularly study the model on a system with zig-zag boundaries along one of the directions. Our two main results are as follows: 1) The system harbors a non-chiral, stationary edge mode at the zig-zag edges (Fig.2a), in strong contrast to the conventional chiral edge modes of topological phases. Through wave packet dynamics we find that such an edge mode is dynamically stabilised even at late times under certain conditions, despite the tendency of the self-acceleration term to diffuse it into the bulk((Fig.2b)). 2) There is a controlled proliferation of pairs of EPs in the Brillouin zone(BZ) within a small bandwidth of the real energy, as the non-reciprocity is tuned. Due to this, the number of EP-pairs in the BZ

keeps jumping by factor of two at certain ‘critical’ values, that gives rise to an intriguing step-like structure as shown in Fig.2c. Further, for a system on a torus, we show that the Berry curvature is completely confined within the ERs and vanishes outside them. Such Berry curvature flux tubes(BCF) could lead to interesting transport signatures. These results position the non-reciprocal NNN Haldane model as a particularly promising system for further investigations.

The paper is organized as follows. In Section II, we introduce the model and discuss its spectral properties, underlying symmetries, ERs, and Berry curvature characteristics. In Section III, we analyse the system under open boundary conditions in a cylindrical geometry with zigzag edges, analyzing the energy spectrum, edge states and exceptional points. In Section IV we study the wave packet dynamics and the dynamical stability of the edge modes. We also study the late-time behaviour of the modes encapsulated between the EPs. Finally, we summarize our results and present concluding remarks in Section V.

II. NON-RECIPROCAL NNN HALDANE MODEL

We consider a tight binding Hamiltonian on a two-dimensional honeycomb lattice with both NN hopping and NNN hopping. The phase in the NNN hoppings of the Haldane model is interpreted as an effective hopping amplitude in the presence of a magnetic flux (though the net flux through the system is zero). In the same spirit, the non-reciprocity in tight-binding hoppings can be re-written effectively as hopping in the presence of an

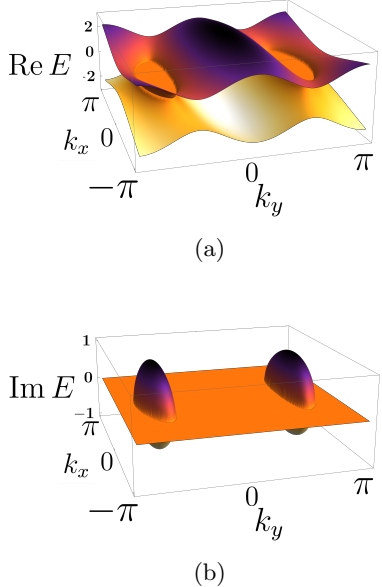


FIG. 3: (a),(b) Real and imaginary parts of the complex energy spectrum under periodic boundary conditions for a system on a torus. We have used $t_1 = 1.0$, $\tilde{t} = 0.22$, $\phi = 0.8$. There are two exceptional rings in the spectrum that mark the transition from \mathcal{PT} -symmetry broken regions, with degenerate real parts and purely imaginary parts, to \mathcal{PT} -symmetric regions with purely real spectrum.

imaginary flux [55, 56]. The resulting Hamiltonian for the ‘imaginary-flux’ Haldane model is then given by

$$\mathcal{H}_{\text{NH-Haldane}} = t_1 \sum_{\langle i,j \rangle} c_i^\dagger c_j + \sum_{\langle\langle i,j \rangle\rangle} \tilde{t} (e^{-\phi} c_i^\dagger c_j + e^{\phi} c_j^\dagger c_i) \quad (1)$$

where $\langle i,j \rangle$ ($\langle\langle i,j \rangle\rangle$) and t_1 (\tilde{t}) denote pairs of NN(NNN) sites and the hopping amplitudes between them respectively (Fig. 1a). The exact mapping between the non-reciprocal hopping and hopping under ‘imaginary-flux’ is as follows: $\tilde{t} e^{\pm\phi} = t_2 \pm \gamma$, where t_2 is usual NNN hopping, $\tilde{t} = \sqrt{t_2^2 - \gamma^2}$ and $\phi = \frac{1}{2} \ln \left(\frac{t_2 - \gamma}{t_2 + \gamma} \right)$. Note that one can go beyond this mapping between non-reciprocal hopping and imaginary flux, and in general treat \tilde{t} and ϕ as independent variables. We would only prefer to be within the constraint of $\tilde{t} e^\phi < t_1$.

Using the periodic boundary conditions imposed along both spatial directions, the Fourier transformed Hamiltonian is expressed as:

$$H(\vec{k}) = \sum_{i=0}^3 h_i(\vec{k}) \sigma_i, \quad (2)$$

$$h_0(\vec{k}) = 2\tilde{t} \cosh \phi \left[\cos(\vec{k} \cdot \vec{a}_1) + \cos(\vec{k} \cdot \vec{a}_2) + \cos(\vec{k} \cdot (\vec{a}_1 - \vec{a}_2)) \right],$$

$$h_1(\vec{k}) = t_1 \left[1 + \cos(\vec{k} \cdot \vec{a}_1) + \cos(\vec{k} \cdot \vec{a}_2) \right],$$

$$h_2(\vec{k}) = t_1 \left[\sin(\vec{k} \cdot \vec{a}_1) + \sin(\vec{k} \cdot \vec{a}_2) \right],$$

$$h_3(\vec{k}) = 2i\tilde{t} \sinh \phi \left[\sin(\vec{k} \cdot \vec{a}_1) - \sin(\vec{k} \cdot \vec{a}_2) - \sin(\vec{k} \cdot (\vec{a}_1 - \vec{a}_2)) \right].$$

As one can see, the imaginary-flux term adds an ‘imaginary Haldane mass term’ to the graphene Hamiltonian. The system respects time-reversal symmetry (TRS) acting on the Bloch Hamiltonian as $H^*(\vec{k}) = H(-\vec{k})$. The imaginary mass-like term generated by the non-reciprocal NNN hopping explicitly breaks chiral symmetry, which is defined as $\Gamma H^\dagger(\vec{k}) \Gamma^{-1} = -H(\vec{k})$.

The flux associated with NNN hopping can in general be made complex leading to a mass term with a function of the form $2i\tilde{t} \sin(\Phi + i\phi)$. In this complex-flux parameter plane, the Haldane model lies on the real axis and our model lies on the imaginary axis. The general complex-flux model is a non-Hermitian extension of the Hermitian Haldane model, breaking the time-reversal symmetry and has gapped edge states with lifetimes [33] (See Appendix C). We are particularly interested in the imaginary-flux model which is a singular limit in the parameter space in that it corresponds to an ‘exceptional phase’ and has time-reversal symmetry protected exceptional rings in the spectrum.

We observe the emergence of a pair of exceptional rings (ERs), i.e. closed loci of exceptional points in the BZ, as shown in Fig. 2. Exceptional points correspond to the simultaneous coalescence of eigenvalues and eigenvectors of a non-Hermitian Hamiltonian, rendering it defective. The ERs are seen to form around the special points K, K' in the Brillouin zone of the hexagonal lattice. It is typically seen that addition of non-Hermiticity to models having degeneracies or avoided crossings lead to formation of exceptional points [35, 57]. In our context, the addition of a time-reversal symmetry protecting imaginary-Haldane term turns the gapless points of Graphene at K, K' to ERs.

The region enclosed by the ERs corresponds to the \mathcal{PT} symmetry broken phase, characterized by complex eigenvalues, while \mathcal{PT} symmetry remains unbroken elsewhere in the BZ, yielding a purely real spectrum despite the non-Hermitian nature of the Hamiltonian [58]. In this model, the ERs mark the transition between unbroken and broken \mathcal{PT} symmetric regions of the spectrum, which is further characterized by the invariant $\text{sgn}[\det H]$ [39, 59] (Fig. 4a).

An interesting feature of the ERs in our model is the landscape of the Berry curvature $\mathbf{B}_n(\vec{k}) = \nabla_{\vec{k}} \times \mathbf{A}_n(\vec{k})$ (between right eigenstates) in the BZ, where Berry connection $\mathbf{A}_n(\vec{k}) = -i \langle u_{n\vec{k}}^R | \nabla_{\vec{k}} | u_{n\vec{k}}^R \rangle$. As shown in Fig. 4b, one can notice that the Berry curvature is completely localised inside the ERs and zero elsewhere. Thus ERs act

as BCF tubes, which is in strong contrast with the distributed Berry curvature landspace, for example in the complex-flux Haldane model (Fig. 10c). We also note that one finds the BCF tube in a model where the Haldane term is replaced by an imaginary Semenoff mass term $\pm iM$. The key difference is that the sign of the Berry curvature in the two ERs have opposite signs as opposed to the case of imaginary flux model (See Appendix C, Fig. 9a). Localised Berry curvature have consequences in the transport properties of the model as we discuss in the final section. In the next section, we consider the consequences for the system with zig-zag boundaries.

III. SYSTEM WITH ZIG-ZAG BOUNDARIES: EDGE-STATES AND NESTED EXCEPTIONAL POINTS

We consider the model under open boundary conditions along one edge and periodic boundary conditions in the other, effectively putting it on a cylinder such that it exhibits zig-zag edges. The simple graphene Hamiltonian with nearest-neighbour hoppings gives rise to gapless edge states at zig-zag boundaries characterized by Zak phase [60]. On the other hand, armchair edges do not have such edge states. We focus on zigzag boundaries, which in our model also give rise to edge-states and exceptional points. The Hamiltonian of the system with zigzag boundaries (periodic along x and open along y) is given by:

$$H(k_x) = \sum_{i=1}^{N_y} \psi_i^\dagger h_{i,i}(k_x) \psi_i + \sum_{i=1}^{N_y-1} \left[\psi_i^\dagger h_{i,i-1}(k_x) \psi_{i-1} + \psi_i^\dagger h_{i,i+1}(k_x) \psi_{i+1} + \text{h.c.} \right] \quad (3)$$

$$\begin{aligned} h_{i,i}(k_x) &= \left[\tilde{t} \cos(k_x - i\phi) + \tilde{t} \cos(k_x + i\phi) \right] \mathbb{I} \\ &\quad + \left[\tilde{t} \cos(k_x - i\phi) - \tilde{t} \cos(k_x + i\phi) \right] \sigma_z \\ &\quad + 2t_1 \cos\left(\frac{k_x}{2}\right) \sigma_x, \\ h_{i,i+1}(k_x) &= \left[\tilde{t} \cos\left(\frac{k_x}{2} + i\phi\right) + \tilde{t} \cos\left(\frac{k_x}{2} - i\phi\right) \right] \mathbb{I} \\ &\quad + \left[\tilde{t} \cos\left(\frac{k_x}{2} + i\phi\right) - \tilde{t} \cos\left(\frac{k_x}{2} - i\phi\right) \right] \sigma_z \\ &\quad + t_1 \sigma^-, \\ h_{i,i-1}(k_x) &= h_{i,i+1}^\dagger(k_x) \end{aligned} \quad (4)$$

where k_x is the momentum along the x -direction. (Note that we have switched from $k_x \in [-\pi, \pi]$ to $k_x \in [0, 2\pi]$ for better visual representation of the EPs in the plots.) Under $i\phi \rightarrow \Phi$, the Hamiltonian matches the Haldane Hamiltonian under zig-zag boundary conditions, whose edge states have been well studied [61, 62]. As we shall see, the edge phenomenology in the imaginary-flux case significantly differs from the Haldane model.

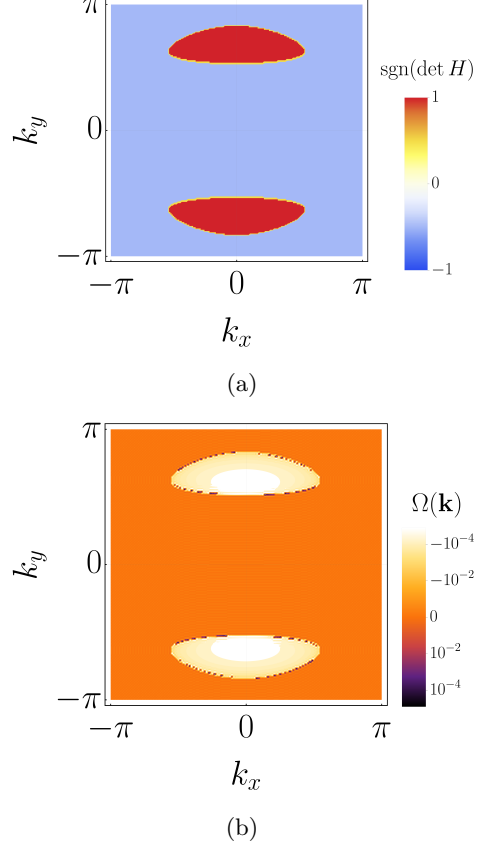


FIG. 4: (a) Sign of the determinant of the Hamiltonian, $\text{sgn}(\det H)$ plotted over the BZ. This invariant distinguishes the \mathcal{PT} symmetry unbroken and \mathcal{PT} symmetry broken regions of the spectrum. The exceptional rings (ERs) mark the boundaries across which the \mathcal{PT} symmetry-breaking transition occurs. (b) Berry-curvature landscape in the presence of ERs. The ERs act as Berry-curvature flux tubes, leading to strong localization of the Berry curvature within their interior. Also, both ERs have the same sign for the Berry curvature.

A. Edge states

Let us now systematically study the impact of non-Hermiticity on the model and analyze the edge-state structure. We first consider the system with a small imaginary flux ϕ introduced through non-reciprocal NNN hopping $\gamma \ll t_2$. This system exhibits complex spectrum as highlighted in Fig. 5(a,b). Each point in the spectrum is colored on the basis of the probability density at one of the edges(left edge). The inverse-participation ratio for a right-eigenstate $|\psi_R\rangle$ $\text{IPR} = \sum_i |\psi_{R,i}|^4 / \sum_i |\psi_{R,i}|^2$, (i is the position index) is also plotted in Fig. 5(c). As can be seen, the edge state occurs at $k_x = \pi$. The notable properties of the edge states are as follows: The dispersion of the edge states, upto quadratic terms, close to $k_x = \pi$ is $E_{\text{edge}}(k_x) = -2\tilde{t} \cosh \phi + \tilde{t} \cosh \phi (k_x - \pi)^2 + 2i\tilde{t} \sinh \phi (k_x - \pi) + \mathcal{O}((k_x - \pi)^3)$.

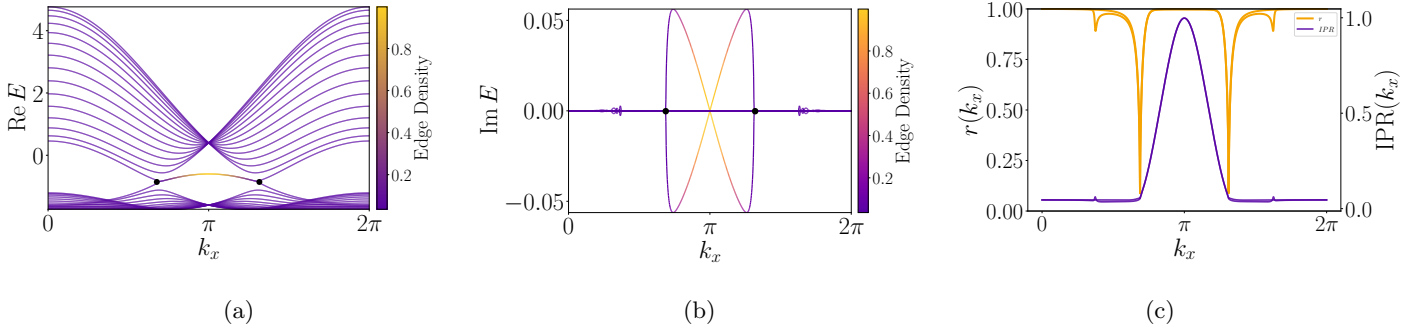


FIG. 5: (a), (b) Spectrum of imaginary-flux Haldane model on a cylinder with zig-zag boundaries. Here, we have, $N_y = 30$, $t_1 = 1$, $t = 0.3$, $\phi = 0.1$. The edge-localized states are highlighted through a color profile by plotting the probability density at the left edge for each state. Non-chiral edge states occur at $k_x = \pi$ with $\partial(\text{Re } E)/\partial k_x = 0$ and $\partial(\text{Im } E)/\partial k_x = \text{constant}$. The edge states merge with the bulk through exceptional points(indicated as black dots) (c) Phase rigidity and the inverse participation ratio(IPR) of the edge states as function of k_x . The phase rigidity goes to zero at the exceptional points, accompanied by IPR also going to zero signalling delocalisation into the bulk.

π)³). As opposed to the Haldane model, the real-part of the dispersion of the edge states shows no chirality at $k_x = \pi$ i.e $\text{Re}(\partial E/\partial k_x) \sim 0$ and has very small dispersion even away from it. On the other hand, the imaginary part of the edge-state spectrum is linear in k_x close to $k_x = \pi$. We will see in Sec.IV that the “chirality” in the imaginary part has consequences in the wave packet dynamics. The black points in Fig.5(a,b) represent EPs where the edge states merge into the bulk through a bifurcation transition. The EPs are signalled by the phase rigidity defined as $r = |\langle \psi_L | \psi_R \rangle| / \sqrt{\langle \psi_L | \psi_L \rangle \langle \psi_R | \psi_R \rangle}$ [63, 64] going to zero as seen in Fig. 5(c). The IPR is also seen to go to zero exactly at those points indicating delocalisation into the bulk.

We study the de-localisation transition of the edge states using the transfer matrix method (Appendix B). This transition is detected by the behaviour of the eigenvalues λ_i of the transfer matrix changing from $|\lambda_i| < 1$ to $|\lambda_i| > 1$. We also reproduce the edge spectrum in the regime of localisation. (Please see Appendix B, Fig.9b). The topological properties of the edge states are also significantly different than that of the Haldane model. Because the time-reversal symmetry is preserved, one does not have full protected topological edge-states in the gap, even though there is edge-localisation. One can compute the winding number treating the system as effective one-dimensional model at each value of k_x (See Appendix B). We find that the winding number is quantised only at $k_x = \pi$ thus leading to a protected edge state at that point. Away from $k_x = \pi$ the winding number is not quantised but will have to be characterised differently as also seen in the case of Rice-Mele and other models [65–67].

Finally, we also numerically study the full lattice Hamiltonian on a cylinder without going to Fourier space and solve for the edge modes. The edge density profile is plotted over the system as shown in Fig.2c.

B. Nested exceptional points of the bulk states:

In the previous section, we discussed how a small imaginary flux leads to the emergence of EPs at the bifurcation points of the edge states. We now turn to the behavior of the bulk states at larger imaginary flux. As shown in Fig. 6a, there are pairs of bulk eigenvalues, which are purely real and lie close to the real part of the edge-state energy from above and below. As the flux is increased they approach one another. Since time-reversal symmetry is preserved, these states are allowed to become degenerate as the flux is increased. However the non-Hermitian nature of the system converts these degeneracies into exceptional points Fig. 6b. Avoided level-crossings or Hermitian degeneracies are typically known to lead to exceptional points upon adding non-Hermiticity[35, 57].

We further study the evolution of the number of EP pairs by increasing the flux ϕ . The number of EP pairs in the spectrum as function of ϕ exhibit a step-like pattern (See Fig.2c). Even a small non-zero flux leads to formation of the first pair of EPs, which are the bifurcation points of the edge states. This pair of EPs persists for a significant interval of ϕ leading to the first plateau. Upon reaching a certain value of flux, the system undergoes an abrupt transition where four more states within the bulk spectrum transform into two pairs of EPs (Fig.6b), thus giving rise to the above stated step-like jump. The point at which the EPs are formed is related to the value of ϕ that was required to bring the two bulk states close to each other. A similar mechanism repeats at another higher value of ϕ where four more bulk states are transformed into EPs (Fig.6c). As a result, the number of EP pairs increases in discrete steps as a function of ϕ . All the EP's are nested within the region between the edge-EPs, thus forming a ‘Matryoshka’(Russian doll) kind of a structure of nested EPs. This can be visually seen particularly in the imaginary part of the energies (Fig.6d).

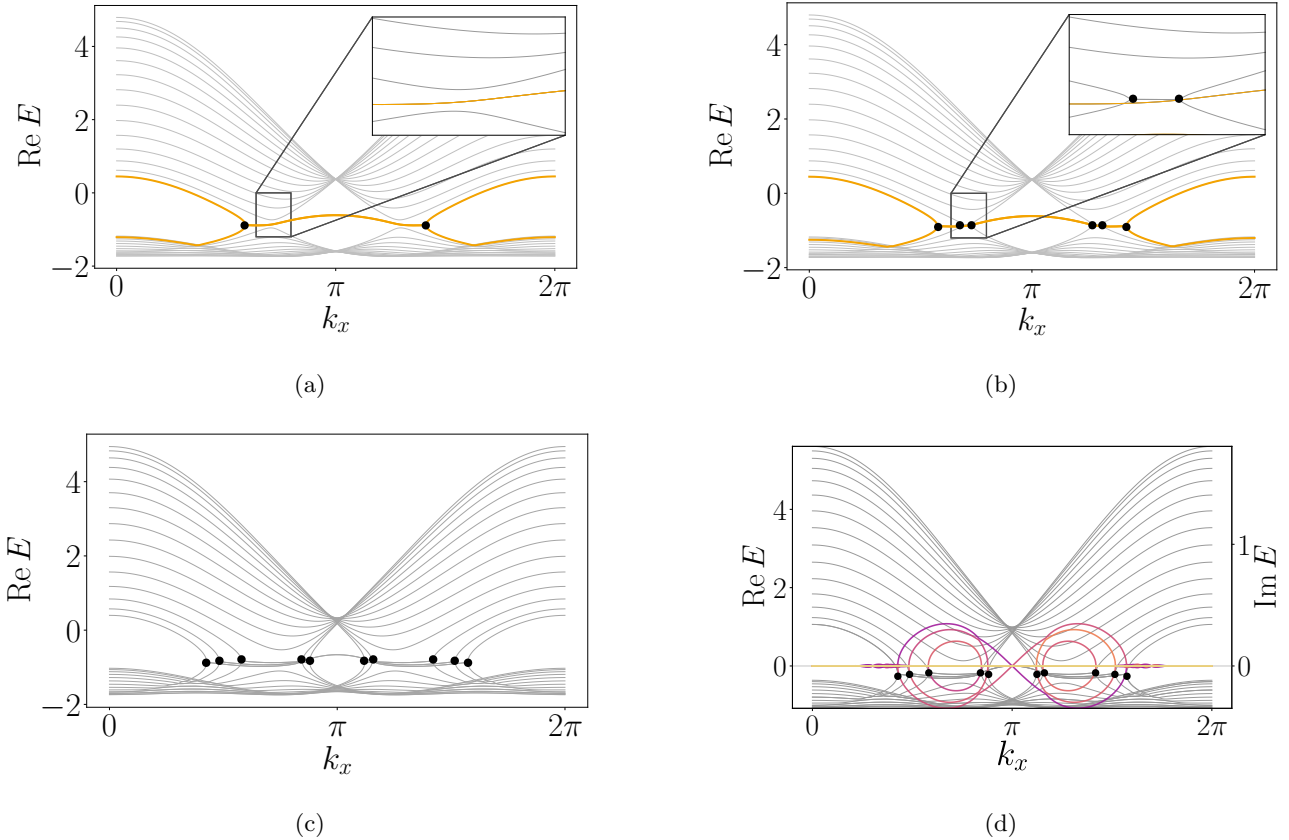


FIG. 6: Proliferation of exceptional points (EPs) with increase in the non-Hermiticity parameter ϕ in the bulk spectrum for system on cylinder with zigzag boundaries. Parameters: $N_y = 30$, $t_1 = 1.0$, and $\tilde{t} = 0.3$. (a) Real part of bulk bands adjacent to the edge bands approach each other as ϕ is increased ($\phi = 0.18$). (b) The bands coalesce giving rise to the formation of two bulk EP pairs ($\phi = 0.2$). (c),(d) Further increase in ϕ leads to proliferation of multiple EP pairs across the spectrum ($\phi = 0.45$). In the imaginary part of the spectrum one can observe the EPs to organize into nested Russian-doll (Matryoshka) like structure arising from successive bulk band coalescences.

The region between the pairs of EPs harbor degenerate states (in real energy) with maximal/minimal imaginary parts. Such bulk states between the EPs survive in the late-time dynamics. We later discuss the late-time wave packet dynamics of such states in Sec. A. The exact mechanism of formation of EPs and determination of the ‘critical’ values of ϕ at which EPs are formed are beyond the scope of this work. This completes our discussion of the edge state and exceptional point properties of the ‘imaginary flux’ Haldane model with zig-zag edges.

IV. WAVE PACKET DYNAMICS AND STEADY-STATE BEHAVIOUR

In this section, we study the wave packet dynamics to better understand how the non-Hermitian spectral properties manifest in the steady state behavior of the system. In studying the wave packet dynamics, we are particularly interested in the scenario of edge-localisation or the lack of it.

We consider a wave packet built from a subset of the bands $|\psi_{R,m}(k_x, y)\rangle$, weighted by a Gaussian distribution function in the k_x space: $w(k_x) = \frac{1}{\sqrt{2\pi\sigma_k^2}} \exp[-(k_x - k_0)^2/(2\sigma_k^2)]$. The time-evolved wave packet is given by $\Psi(y, t) = \sum_m \int dk_x e^{-iE_m(k_x)t} w(k_x) |\psi_{R,m}(k_x, y)\rangle$, where $|\psi_{R,m}(k_x, y)\rangle$ is the m -th right-eigenvector. The center k_0 and the width σ_k are chosen so as to pick the states of interest in the BZ. The summation in the wave packet is over a sub-set of bands, typically chosen to be one of the edge states or a bulk band hosting a pair of EPs. The equations of motion for the wave packet center along the periodic direction x and the corresponding transverse momentum space k_x are given by [33, 68, 69]: $\langle \dot{x} \rangle = \frac{d \operatorname{Re} E_k}{dk_x}$ and $\langle \dot{k}_x \rangle = \sigma_k^2 \frac{d \operatorname{Im} E_k}{dk_x}$. While the velocity $\langle \dot{x} \rangle$ is given by the usual Ehrenfest equation, the ‘self-acceleration’ $\langle \dot{k}_x \rangle$ is dictated by the slope of imaginary part of the spectrum and also the width of the wave packet.

In order to study the edge-state dynamics, we initialize a wave packet that is centered around $k_x =$

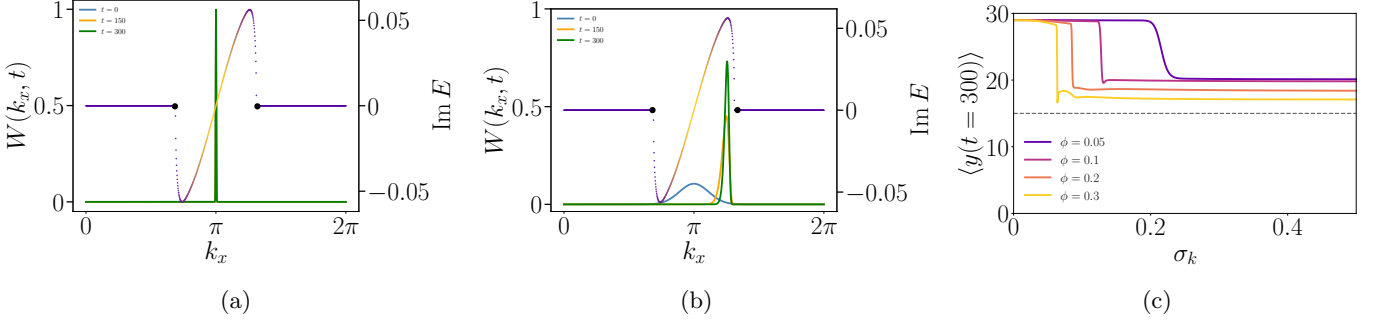


FIG. 7: (a),(b) Dynamics of the wave packet distribution $W(k_x, t)$ for an edge band at small non-Hermiticity $\phi = 0.05$. Other parameters are $N_y = 30$, $t_1 = 1.0$, $\tilde{t} = 0.3$. (a) A highly localized $W(k_x, t)$ around $k_x = \pi$ with width $\sigma_k = 0.01$ does not experience a self-acceleration $\langle \dot{k} \rangle$ induced drift. As a result it persists at the edge even at late-times. (b) A broader distribution $W(k_x, t)$ with $\sigma_k = 0.5$ experiences the self acceleration and moves away from $k_x = \pi$. As it approaches the maximum of the imaginary part, it loses the edge localisation along y and diffuses into the bulk. (c) Width-tolerance window for late-time edge-stabilisation progressively narrows for comparatively higher values of non-Hermiticity. But as the non-Hermiticity is decreased one can see that the tolerance window widens. (Note that the relevant scale for comparing wavepacket widths is approximately set by the momentum-space separation between the exceptional points.)

π and therefore localised at the edges $y = 0$ or $y = N_y$ in real space. We also track the motion of the wave packet distribution in k_x space by plotting $W(k_x, t) = |\langle \psi_{L,n}(k_x) | \Psi(y, t) \rangle|^2 = |e^{-iE_n(k_x)t} w(k_x)|^2$, where $|\psi_{L,n}(k_x)\rangle$ is the left-eigenvector. We provide an analytical derivation of the behaviour of $W(k_x, t)$ particularly for the edge states in Appendix A. We also compute $\langle y(t) \rangle$ to track the edge-localisation properties at late times.

The key features of the edge wave packet dynamics are as follows : 1) Because of the vanishing slope in the real spectrum at $k_x = \pi$, the edge mode wave packet is stationary along the transverse direction, in contrast to the conventional chiral edge modes in topological phases. 2) The finite slope in the imaginary spectrum $v_I = (\partial \text{Im} E) / \partial k_x|_{k_x=\pi}$ gives rise to a ‘self-acceleration’ in the edge wave packet. An interplay between the motion of the wave packet and the localisation landscape in the k_x -space, dictates the late-time localisation properties of the wave packet along y -direction. Particularly in the case of the edge band, the states close to $k_x = \pi$ are highly edge-localised and they delocalise as we move towards EPs (Fig.5). The wave packet moves away from $k_x = \pi$ as $k_x(t) = k_0 + v_I \sigma_k^2 t$. Consequently, in real space, it diffuses into the bulk along the y -axis, thus losing the edge-localisation and becoming an ‘ephemeral edge mode’ (Fig.7a, 7b). We further uncover a parameter regime where the ephemeral edge modes can be stabilised for longer time scales. Note that the slope of the imaginary dispersion is $v_I \sim \tilde{t} \sinh \phi$. Therefore, for very small non-hermiticity $\phi \ll 1$ (implies $v_I \ll 1$), and for a range of small wave packet widths, the initial ‘drift’ $v_I \sigma_k^2 t$ is extremely small. This leads to negligible a diffusion into the bulk and stabilisation at the edge at longer times, as seen in Fig.2b. The width-tolerance for

late-time edge stabilisation drops as we increase the non-hermiticity (Fig.7c). The small non-reciprocity, for example $\phi = 0.05$ that we have chosen in Fig.7, would imply $t_2 = 0.3003, \gamma = 0.015$, which is a physically reasonable non-Hermitian deviation from a Hermitian model. In the following, we study the effect of different wavepacket widths on the late-time dynamics. The relevant scale for comparing wavepacket widths is approximately set by the momentum-space separation between the exceptional points, where the imaginary part has a finite dispersion.

To further understand this, let us start with a narrow wave packet centered at $k_x = \pi$ ($\sigma_k \ll 1$, $\langle \dot{k}_x \rangle \sim 0$) (Fig.7a). Such a wave packet undergoes negligible drift in k_x and will remain stationary around $k_x = \pi$ even at late times. In the real space, this would mean that the wave packet remains highly localised at the edge as seen in behaviour of $\langle y(t) \rangle$ in Fig.2b. One can also choose a sufficiently wider wave packet at smaller $\phi \ll 1$ to get such an edge stabilisation (Fig.7c). For larger ϕ , a wider wave packet has a finite self-acceleration $\langle \dot{k}_x \rangle$ and drifts away from $k_x = \pi$ until it reaches a steady-state at the maximum of the dispersion, where the slope of $\text{Im} E_k$ vanishes (Fig.7b). The maximum in the imaginary dispersion acts as a basin of the steady states in the sense that any wider width wave packet converges to that point at different rates (Fig.7c). The states around the maxima are delocalised but nevertheless have a finite but small polarisation away from the center. This gives rise to a dynamical diffusion into the bulk yet shifted away from the center at steady state (Fig.2b, 7c). Such a diffusion from the edge to the bulk has been reported in recent works as well [69–71]. We have thus demonstrated that the imaginary-flux Haldane model harbors ‘ephemeral’ non-chiral modes, whose lifetimes can be tuned based on the the non-hermiticity and wave packet widths. In the

Appendix A, we show how maxima of the imaginary dispersion that occurs between the proliferated EPs formed by the bulk states, also act as a basin of steady states.

V. CONCLUSION AND DISCUSSION

We have studied the ‘exceptional phase’ of the imaginary-flux Haldane model that hosts TRS protected ERs and edge states localised at the zig-zag boundaries on a cylinder. Our primary finding is the existence of a ‘non-chiral’ edge mode at $k_x = \pi$. We found that in the regime of small non-hermiticity, the wave packet initialised at the edge will remain stationary, with very small diffusion into the bulk. Such a non-chiral edge localisation is in contrast to the chiral modes found in topological phases. The self-acceleration term in the equations of motion leads to diffusion of the edge wavepacket into the bulk, thus making them ‘ephemeral edge modes’. The lifetime of bulk-diffusion can be tuned based on the non-Hermiticity and wave packet width.

The imaginary-flux Haldane model is also an example of a lattice model in two dimensions that harbors ERs, while most other studies have focused on continuum models. The ERs are also known to exhibit non-linear Hall responses as has been explored in continuum systems [53]. Given that in our model the sign of the Berry curvature does not change in both the ERs, as opposed to the imaginary mass model, this could lead to absence of cancellations upon integrating around the BZ and a finite total transport response [72]. ERs also emerge in the Majorana-basis Haldane model that appears in the context of disordered Kitaev honeycomb model [54]. In that setting, our results would imply a non-chiral Majorana edge mode, which would be of immense interest. Further, it will be interesting to study the consequences of the exceptional and edge physics translated to spin-language of the Kitaev honeycomb model. One could also investigate other mechanisms to stabilise the diffusive edge modes for longer times.

We also found step-like jumps in the number of EP-pairs that are accumulated as the non-hermiticity is tuned. Another investigation for future is to understand the exact mechanism of proliferation of the bulk EPs and to estimate the values at which they are formed in Fig.2c, which will help us explain the step-like structure. One can also investigate how the step-like EP cascading explicitly appears as a signature in any physical phenomena. Thus we have brought forth the imaginary-flux Haldane model as a simple model to explore many exceptional point realted effects and edge physics. It further warrants investigations into its experimental realization on top of already proposed ones in optical and topoelectric circuits[26, 33]. It would also be interesting to understand the ‘singular’ exceptional nature of the imaginary-flux model in the full parameter space of the complex flux Haldane model.

ACKNOWLEDGMENTS

SH would like to acknowledge funding support from the ANRF Prime Minister Early Career Grant(PM-ECRG): ANRF/ECRG/2024/002083/PMS. AP acknowledges the Institute Fellowship from the Indian Institute of Science Education and Research, Thiruvananthapuram (IISER TVM). Both AP and HC acknowledge institutional support and research facilities provided by IISER TVM.

Appendix A: Wave packet distribution in k_x space and dynamics of bulk states

In this appendix, we obtain the behaviour of the wave packet distribution $W(k_x, t)$. This will help us track its motion in k_x as the wave packet evolves.

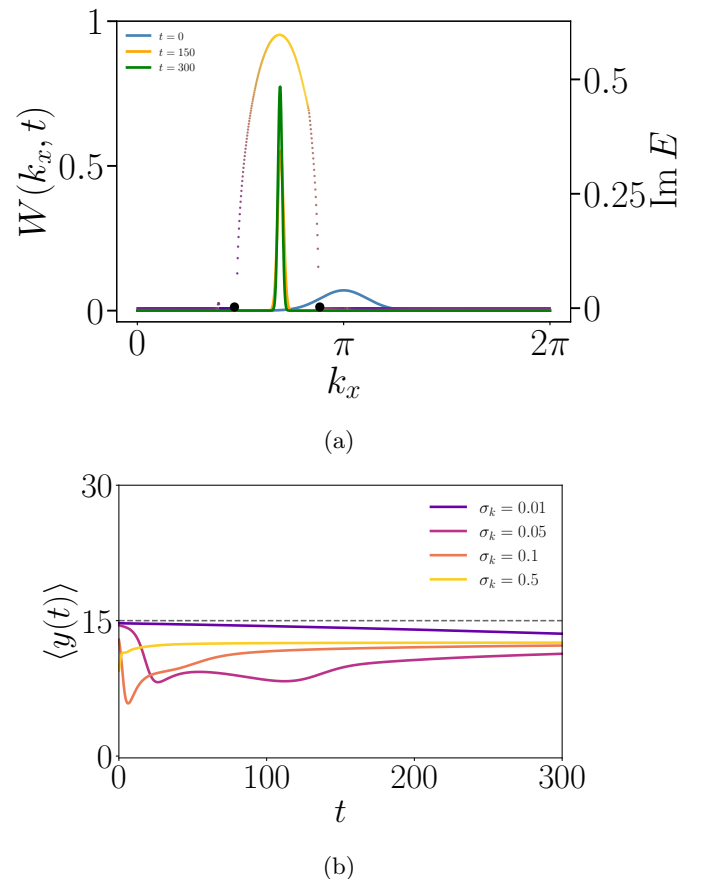


FIG. 8: (a) Wavepacket distribution dynamics for a bulk band with two exceptional points. An initial wavepacket around an exceptional point evolves and as a steady-state settles at the maximum of the imaginary part. (b) Expectation value of evolved over time with different widths of wave packet over a bulk band with $\phi = 0.45$. The late-time value $y(t)$ is shifted off the center of the system indicating the polarized nature of the states at the maximum of the imaginary spectrum.

The wave packet distribution is given by $W(k_x, t) = |\langle \psi_{L,m}(k_x) | \Psi(y, t) \rangle|^2 = |e^{-iE_m(k_x)t} w(k_x)|^2$, where the relevant terms are defined in the main text. We are particularly interested in the behaviour for the edge band $E_m = E_{EB}$. Using $|e^{-iE_{EB}t}|^2 = e^{2\text{Im}(E_{EB})t}$, we get

$$W(k_x, t) \approx \exp \left[-\frac{(k_x - k_0)^2}{\sigma_k^2} + 2 \text{Im} E_{EB}(k_x) t \right]. \quad (\text{A1})$$

Expanding to linear order around $k_x = \pi$, we get $\text{Im} E_{EB}(k_x) = v_I(k_x - \pi)$ where $v_I = (\partial \text{Im} E_{EB}) / \partial k_x|_{k_x=\pi}$. Substituting into $W(k_x, t)$ and completing the squares,

$$W(k_x, t) \approx \left(e^{v_I^2 \sigma_k^2 t^2} \right) \exp \left[-\frac{(k_x - k_0 - v_I \sigma_k^2 t)^2}{\sigma_k^2} \right]. \quad (\text{A2})$$

Thus, the center of the Gaussian moves as $k_x(t) = k_0 + v_I \sigma_k^2 t$, which is nothing but a solution of the equation of motion: $\langle \dot{k}_x \rangle = v_I \sigma_k^2$, assuming v_I is not a function of k_x , which is valid around $k_x = \pi$. At the same time, the additional exponential factor in front of the Gaussian will amplify the wave packet amplitude as a function of time. In a more general case i.e away from $k_x = \pi$ and for other bands such as the ones with a pair of bulk exceptional points, the motion of the wave packet follows $k_x = \sigma_k^2 \frac{\partial \text{Im} E}{\partial k_x}$. Here we also discuss the dynamics for a wave packet constructed out of the states that are encapsulated by the bulk EPs. As in the case of the edge band, there exists a maxima in the imaginary part of the dispersion for these states (Fig.8 (a)). The wave packet moves in k_x until it hits the maximum of the imaginary dispersion, where the slope vanishes. After that instant, the wave packet stops moving and samples only the states around the maximum imaginary point. Therefore the maximum of imaginary part of the spectrum for any band acts as a basin of steady states. The states around the maxima are special from the view of their localisation properties along y . These states are delocalised into the bulk along y but have a small polarisation away from the center. Therefore, “center of mass” $\langle y(t) \rangle$ converges to a steady state value that is shifted away from the center of the system as illustrated in Fig.8.

Appendix B: Transfer-matrix and Winding number analysis

Transfer Matrix analysis: In this section, we analyze the edge mode wavefunction and spectrum using the transfer-matrix method. The formalism employed here closely follows the general framework developed in Ref. [73], which we adapt to the present non-Hermitian model. Under zig-zag boundary conditions the Hamiltonian is given by Eq.(4). By writing the edge mode as $\Psi(k_x)_{\text{Edge}}^\dagger = \sum_i^{N_y} \psi_i(k_x)^\dagger \phi_i$, the equation of the motion gives the following recurrence relation

$$A\phi_{i+1} + A^\dagger \phi_{i-1} + B\phi_i = E(k_x)\phi_i, \quad (\text{B1})$$

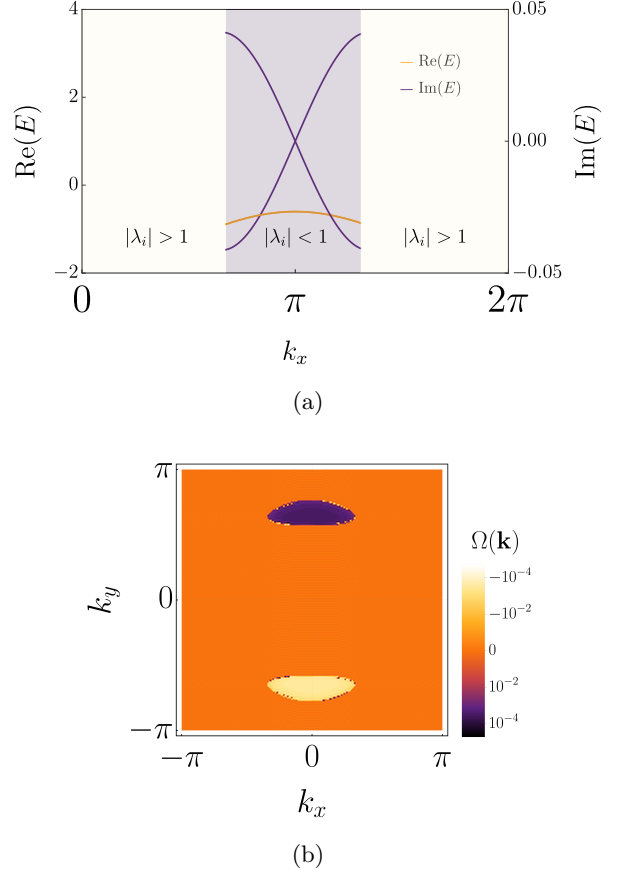


FIG. 9: (a) Behaviour of the eigenvalues $\{\lambda_i\}$ of transfer matrix for the edge state. A bifurcation transition from edge localisation to bulk delocalisation is signaled by $|\lambda_i| = 1$. The edge spectrum is also obtained by imposing the condition $|\lambda_i| < 1$. (b) Berry curvature plotted over the BZ in the model for Graphene with imaginary Semenoff mass $M = 0.5i$. The Berry curvature is also localised within the exceptional rings in this case, but come with opposite signs between the two exceptional rings.

where ϕ_i denotes the amplitude at the i^{th} site and $h_{i,i} = B(k_x)$, $h_{i,i-1} = A(k_x)$ (to simplify notation). The transfer matrix for the above is given by

$$\begin{pmatrix} \phi_{i+1}(k_x) \\ \phi_i(k_x) \end{pmatrix} = T(k_x) \begin{pmatrix} \phi_i(k_x) \\ \phi_{i-1}(k_x) \end{pmatrix}. \quad (\text{B2})$$

$$T(k_x) = \begin{pmatrix} A^{-1}(k_x)[E(k_x)I_2 - B(k_x)] & -A^{-1}(k_x)A^\dagger(k_x) \\ I_2 & 0 \end{pmatrix}$$

Solving for the eigenvalues $\{\lambda_i\}$ of the transfer matrix [74, 75], we obtain the edge mode spectrum and the parameter range for their existence by imposing the condition $0 < |\lambda_i| < 1$. We see that the range of k_x that has edge-localised states is bounded precisely by the EPs (Fig.9b).

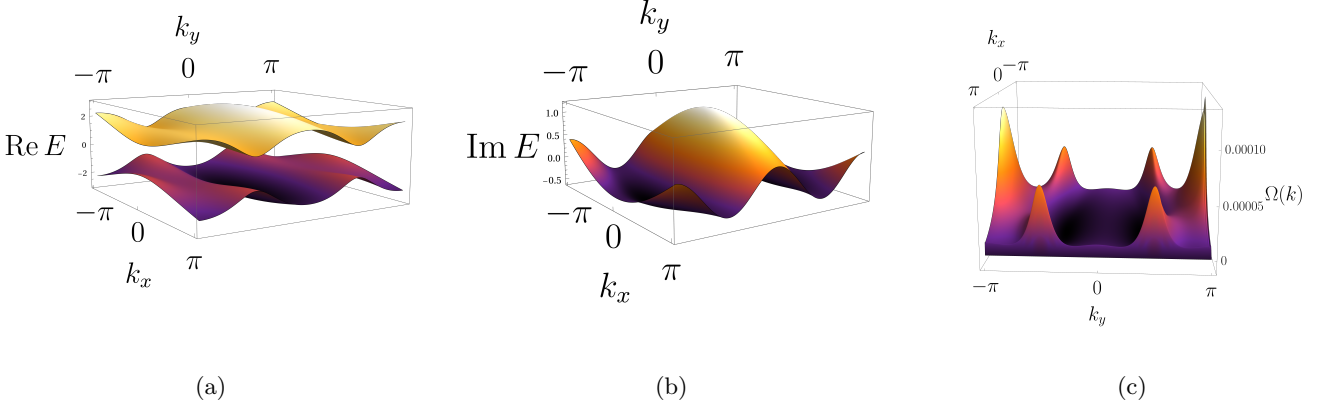


FIG. 10: (a), (b) Real and imaginary parts of the energy spectrum with complex-flux Haldane model under periodic boundary conditions. The real part is gapped and there are no EPs. (c) Berry curvature distribution for right eigenstates of the complex-flux model. Parameters: $t_1 = 1$, $\tilde{t} = 0.22$, $\phi = 0.8$, $\Phi = \pi/2$. The Berry curvature is smoothly distributed over the BZ.

Winding number: There is a winding number associated with the edge mode appearing at $k_x = \pi$. One can reinterpret the Hamiltonian in Eq.3 as a family of 1D Hamiltonians with k_x as an external parameter. Using the framework used to characterise the edge states of the Haldane mode [76], our model can be rewritten as an 1D effective model for each value of k_x (imposing PBC along y).

$$H(k_y) = d_0(k_y) \sigma_0 + d_x(k_y) \sigma_x + d_y(k_y) \sigma_y + d_z(k_y) \sigma_z \quad (\text{B3})$$

where the components of $\mathbf{d}(k_y)$ are $d_0(k_y) = 2\tilde{t} \cosh \phi [\cos k_x + 2 \cos(\frac{k_x}{2}) \cos k_y]$, $d_x(k_y) = t_1 [2 \cos(\frac{k_x}{2}) + \cos k_y]$, $d_y(k_y) = -t_1 \sin k_y$, and $d_z(k_y) = 2i\tilde{t} \sinh \phi [\sin k_x + 2 \sin(\frac{k_x}{2}) \cos k_y]$. The winding number $\nu = (1/2\pi) \int (\hat{d}(k_y) \times d\hat{d}(k_y)/dk_y) \cdot \hat{n} dk_y$ gives a quantised value of ± 1 only at $k_x = \pi$. Interestingly, this is true for any value of the non-Hermitian parameter ϕ . Away from $k_x = \pi$, the edge-localised modes do not have a winding in the above sense, but could be characterised using other means as proposed in the literature [65–67].

Appendix C: Complex-flux Haldane model

In the main text, we introduced a non-Hermitian Haldane model in the presence of background flux that was

purely imaginary. In this appendix, we extend the construction further by promoting the flux to be a fully complex quantity $\Phi + i\phi$:

$$\begin{aligned} \mathcal{H}_{\text{NH Haldane}} = & t_1 \sum_{\langle i,j \rangle} c_i^\dagger c_j + \sum_i M_i c_i^\dagger c_i \\ & + \tilde{t} \sum_{\langle\langle i,j \rangle\rangle} \left[e^{i(\Phi+i\phi)} c_i^\dagger c_j + e^{-i(\Phi+i\phi)} c_j^\dagger c_i \right] \end{aligned} \quad (\text{C1})$$

The model reduces to the usual Haldane model at $\phi = 0$ and $\Phi = \frac{\pi}{2}$. Imposing periodic boundary conditions along both lattice directions allows us to express the Hamiltonian in momentum space as in Eqs. (2) but with a complex flux.

We note that the time-reversal symmetry is preserved only when $\Phi = 0$ and broken for any small finite value of real flux. With broken TRS, in some parameter regimes the model exhibits a ground state with a finite Chern number separated from the other band by a well-defined gap (Figs.10a, 10b). There are chiral edge states on imposing open boundary conditions but with finite life times [33]. We additionally compute the Berry curvature of this model and find that its distribution differs remarkably from that obtained in our system in that it is smoothly distributed throughout the BZ in contrast with the confinement in ERs (See Fig.10c).

We also consider a model with an imaginary Semenoff mass term ($M = \pm i\Gamma$) and no NNN hoppings. Although this model also hosts exceptional rings, its Berry curvature landscape differs from our model. In particular, one can observe from Fig. 9a that the Berry curvature has opposite-signed contributions between the two ERs across the BZ. This could lead to cancellations in quantities when integrated over the BZ.

[1] C.-E. Bardyn, M. A. Baranov, C. V. Kraus, E. Rico, A. İmamoğlu, P. Zoller, and S. Diehl, New Journal of Physics **15**, 085001 (2013).

[2] Y. Ashida, Z. Gong, and M. Ueda, Advances in Physics **69**, 249 (2021).

[3] E. J. Bergholtz, J. C. Budich, and F. K. Kunst, Rev.

Mod. Phys. **93**, 015005 (2021).

[4] K. Ding, C. Fang, and Y. Ma, Nature Reviews Physics **4**, 745 (2022).

[5] M. De Carlo, F. De Leonardis, R. A. Soref, L. Colatorti, and V. M. N. Passaro, Sensors **22**, 3977 (2022).

[6] C. Gneiting, A. Koottandavida, A. V. Rozhkov, and F. Nori, Phys. Rev. Res. **4**, 023036 (2022).

[7] N. Okuma and M. Sato, Annual Review of Condensed Matter Physics **14**, 83 (2023).

[8] V. Meden, L. Grunwald, and D. M. Kennes, Reports on Progress in Physics **86**, 026001 (2023).

[9] K. Sone, K. Yokomizo, K. Kawaguchi, and Y. Ashida, Reports on Progress in Physics **89**, 016501 (2026).

[10] D. V. Savin, V. V. Sokolov, and H.-J. Sommers, Phys. Rev. E **67**, 026215 (2003), shows how non-Hermitian effective Hamiltonians emerge from potentials and resolvents in scattering theory, with Green's function resolvents encoding complex poles.

[11] K. G. Zloshchastiev and A. Sergi, J. Mod. Opt. **61**, 1298 (2014).

[12] S. Echeverri-Arteaga, H. Vinck-Posada, and E. A. Gómez, Optik **180**, 505–510 (2019).

[13] F. Song, S. Yao, and Z. Wang, Phys. Rev. Lett. **123**, 170401 (2019).

[14] A. Altland, M. Fleischhauer, and S. Diehl, Phys. Rev. X **11**, 021037 (2021).

[15] B. Michen, T. Micallo, and J. C. Budich, Phys. Rev. B **104**, 035413 (2021).

[16] A. Purkayastha, Physical Review A **105**, 10.1103/physreva.105.062204 (2022).

[17] C. Lehmann, T. Micallo, and J. C. Budich, Phys. Rev. B **110**, 125426 (2024), shows how an effective non-Hermitian quasiparticle Hamiltonian naturally emerges from Green's function spectral analysis in interacting systems with correlations.

[18] A. Banerjee, R. Sarkar, S. Dey, and A. Narayan, Journal of Physics: Condensed Matter **35**, 333001 (2023).

[19] L. Feng, R. El-Ganainy, and L. Ge, Nature Photonics **11**, 752 (2017).

[20] Y. Takasu, T. Yagami, Y. Ashida, R. Hamazaki, Y. Kuno, and Y. Takahashi, Progress of Theoretical and Experimental Physics **2020** (2020).

[21] H. G. Song, M. Choi, K. Y. Woo, C. H. Park, and Y.-H. Cho, Nature Photonics **15**, 582 (2021).

[22] Z. Lin, L. Zhang, X. Long, Y.-a. Fan, Y. Li, K. Tang, J. Li, X. Nie, T. Xin, X.-J. Liu, and D. Lu, npj Quantum Information **8**, 10.1038/s41534-022-00587-3 (2022).

[23] B. Liu, Y. Li, B. Yang, X. Shen, Y. Yang, Z. H. Hang, and M. Ezawa, Phys. Rev. Research **5**, 043034 (2023).

[24] Z. Li, L.-W. Wang, X. Wang, Z.-K. Lin, G. Ma, and J.-H. Jiang, Nature Communications **15**, 10.1038/s41467-024-50776-1 (2024).

[25] F. D. M. Haldane, Phys. Rev. Lett. **61**, 2015 (1988).

[26] M. Ezawa, Phys. Rev. B **100**, 081401 (2019).

[27] P. Reséndiz-Vázquez, K. Tschernig, A. Pérez-Leija, K. Busch, and R. d. J. León-Montiel, Phys. Rev. Res. **2**, 013387 (2020).

[28] W. Zhu and J. Gong, Phys. Rev. B **106**, 035425 (2022).

[29] C. Wang, T.-C. Yi, J. Li, and R. Mondaini, Phys. Rev. B **108**, 085134 (2023).

[30] M.-S. Wei, Y.-Q. Wang, M.-J. Liao, Y. Yang, and J. Xu, Opt. Express **31**, 39424 (2023).

[31] T. Jiang, C. Zhang, R.-Y. Zhang, Y. Yu, Z. Guan, Z. Wei, Z. Wang, X. Cheng, and C. Chan, Nature Communications **15**, 10863 (2024).

[32] X. Xie, F. Ma, W. B. Rui, Z. Dong, Y. Du, W. Xie, Y. X. Zhao, H. Chen, F. Gao, and H. Xue, Nature Communications **16**, 1627 (2025), note that even though this work claimed to implement non-reciprocal NNN hoppings, the PBC Hamiltonian on a torus presented in their text were erroneous, in that it missed the crucial σ_z term.

[33] W. Dong, Q.-D. Jiang, and M. Baggioli, Non-hermitian wave-packet dynamics and its realization within a non-hermitian chiral cavity (2025), arXiv:2501.12163 [cond-mat.mes-hall].

[34] X.-C. Chen, X.-F. Nie, Y.-W.-Y. Li, and W.-X. Cui, Front. Phys. **13**, 1572883 (2025).

[35] W. D. Heiss, Journal of Physics A: Mathematical and Theoretical **45**, 444016 (2012).

[36] Y. Xu, S.-T. Wang, and L.-M. Duan, Phys. Rev. Lett. **118**, 045701 (2017).

[37] J. Carlström and E. J. Bergholtz, Phys. Rev. A **98**, 042114 (2018).

[38] A. Cerjan, M. Xiao, L. Yuan, and S. Fan, Phys. Rev. B **97**, 075128 (2018).

[39] R. Okugawa and T. Yokoyama, Phys. Rev. B **99**, 041202 (2019).

[40] J. C. Budich, J. Carlström, F. K. Kunst, and E. J. Bergholtz, Phys. Rev. B **99**, 041406 (2019).

[41] K. Moors, A. A. Zyuzin, A. Y. Zyuzin, R. P. Tiwari, and T. L. Schmidt, Phys. Rev. B **99**, 041116 (2019).

[42] H. Wang, J. Ruan, and H. Zhang, Phys. Rev. B **99**, 075130 (2019).

[43] T. Yoshida, R. Peters, N. Kawakami, and Y. Hatsugai, Phys. Rev. B **99**, 121101 (2019).

[44] T. Yoshida and Y. Hatsugai, Phys. Rev. B **100**, 054109 (2019).

[45] H. Wang, B. Xie, S. K. Gupta, X. Zhu, L. Liu, X. Liu, M. Lu, and Y. Chen, Phys. Rev. B **100**, 165134 (2019).

[46] T. Liu, J. J. He, Z. Yang, and F. Nori, Phys. Rev. Lett. **127**, 196801 (2021).

[47] W. B. Rui, M. M. Hirschmann, and A. P. Schnyder, Phys. Rev. B **100**, 245116 (2019).

[48] T. Isobe, T. Yoshida, and Y. Hatsugai, Phys. Rev. B **104**, L121105 (2021).

[49] M. Stålhammar and E. J. Bergholtz, Phys. Rev. B **104**, L201104 (2021).

[50] T. Isobe, T. Yoshida, and Y. Hatsugai, Nanophotonics **12**, 2335 (2023).

[51] Z. Lei and Y. Deng, Communications Physics **8**, 67 (2025).

[52] Y. Huang, Phys. Rev. B **111**, 085120 (2025).

[53] F. Qin, R. Shen, and C. H. Lee, Phys. Rev. B **111**, 245413 (2025).

[54] K. Yang, D. Varjas, E. J. Bergholtz, S. Morampudi, and F. Wilczek, Phys. Rev. Res. **4**, L042025 (2022).

[55] N. Hatano and D. R. Nelson, Phys. Rev. Lett. **77**, 570 (1996).

[56] S. Longhi, Phys. Rev. A **95**, 062122 (2017).

[57] W. D. Heiss and A. L. Sannino, Journal of Physics A: Mathematical and General **23**, 1167 (1990).

[58] C. M. Bender and S. Boettcher, Phys. Rev. Lett. **80**, 5243 (1998).

[59] Z. Gong, Y. Ashida, K. Kawabata, K. Takasan, S. Higashikawa, and M. Ueda, Phys. Rev. X **8**, 031079 (2018).

[60] P. Delplace, D. Ullmo, and G. Montambaux, Phys. Rev. B **84**, 195452 (2011).

[61] N. Hao, P. Zhang, Z. Wang, W. Zhang, and Y. Wang,

Phys. Rev. B **78**, 075438 (2008).

[62] S. Traverso, M. Sassetti, and N. Traverso Ziani, npj Quantum Materials **9**, 10.1038/s41535-023-00615-1 (2024).

[63] D. C. Brody, Journal of Physics A: Mathematical and Theoretical **47**, 035305 (2013).

[64] J. Wiersig, Phys. Rev. Res. **5**, 033042 (2023).

[65] H. Jiang, C. Yang, and S. Chen, Phys. Rev. A **98**, 052116 (2018).

[66] K. Hattori and A. Yamaguchi, Journal of the Physical Society of Japan **93**, 10.7566/jpsj.93.044702 (2024).

[67] J. Zhong, H. Wang, A. N. Poddubny, and S. Fan, Phys. Rev. Lett. **135**, 016601 (2025).

[68] L. Muschietti and C. T. Dum, Physics of Fluids B: Plasma Physics **5**, 1383 (1993).

[69] Y. He and T. Ozawa, Anomalous wave-packet dynamics in one-dimensional non-hermitian lattices (2025), arXiv:2512.07484 [physics.optics].

[70] Z.-Q. Zhang, Y.-H. Ren, M. Lu, and H. Jiang, Phys. Rev. B **112**, 144305 (2025).

[71] S. Jana, B. M. Manda, V. Achilleos, D. J. Frantzeskakis, and L. Sirota, Solution of wave acceleration and non-hermitian jump in nonreciprocal lattices (2025), arXiv:2512.18287 [cond-mat.mes-hall].

[72] Upcoming work by one of the authors.

[73] T. Mizoguchi and T. Koma, Phys. Rev. B **103**, 195310 (2021).

[74] V. Dwivedi and V. Chua, Phys. Rev. B **93**, 134304 (2016).

[75] K. Kawabata, K. Shiozaki, and M. Ueda, Phys. Rev. B **98**, 165148 (2018).

[76] G. Al-Mahmood, M. Amini, E. Ghanbari-Adivi, and M. Soltani, Physica Scripta **101**, 015902 (2026).

[77] T. Micallo, C. Lehmann, and J. C. Budich, Phys. Rev. Res. **5**, 043105 (2023).

[78] R. Sarkar, A. Bandyopadhyay, and A. Narayan, Phys. Rev. B **107**, 035403 (2023).

[79] K. Kawabata, K. Shiozaki, M. Ueda, and M. Sato, Phys. Rev. X **9**, 041015 (2019).

[80] N. Hatano and D. R. Nelson, Phys. Rev. Lett. **77**, 570 (1996).

[81] N. Hatano and D. R. Nelson, Phys. Rev. B **56**, 8651 (1997).

[82] Y. D. Chong, Phys. Rev. B **81**, 052303 (2010).

[83] S. Yao and Z. Wang, Phys. Rev. Lett. **121**, 086803 (2018).

[84] F. K. Kunst, E. Edvardsson, J. C. Budich, and E. J. Bergholtz, Phys. Rev. Lett. **121**, 026808 (2018).

[85] S. Yao and Z. Wang, Phys. Rev. Lett. **121**, 086803 (2018).

[86] K. Yokomizo and S. Murakami, Phys. Rev. Lett. **123**, 066404 (2019).

[87] D. C. Brody, Journal of Physics A: Mathematical and Theoretical **47**, 035305 (2014).

[88] B. Zhen, C. W. Hsu, Y. Igarashi, L. Lu, I. Kaminer, A. Pick, S.-L. Chua, J. Joannopoulos, and M. Soljačić, Nature **525**, 354 (2015).

[89] M. V. Berry, Proceedings of the Royal Society of London. A. Mathematical and Physical Sciences **392**, 45 (1984).

[90] Z. Zhang, I. Septembre, Z. Liu, P. Kokhanchik, S. Liang, F. Liu, C. Li, H. Wang, M. Liu, Y. Zhang, M. Xiao, G. Malpuech, and D. Solnyshkov, Phys. Rev. Lett. **135**, 263802 (2025).

[91] L. Jin and Z. Song, Phys. Rev. B **99**, 081103 (2019).

[92] B. Zhen, C. W. Hsu, Y. Igarashi, L. Lu, I. Kaminer, A. Pick, S.-L. Chua, J. D. Joannopoulos, and M. Soljačić, Nature **525**, 354 (2015).

[93] M. Parto, Y. G. N. Liu, B. Bahari, M. Khajavikhan, and D. N. Christodoulides, Nanophotonics **10**, 403 (2021).

[94] B. Zhen, C. W. Hsu, Y. Igarashi, L. Lu, I. Kaminer, A. Pick, S.-L. Chua, J. D. Joannopoulos, and M. Soljačić, Nature **525**, 354 (2015).